Abdeldjabar Benrabah[1, *], Farid Khoucha[1], Ali Raza[2], Dianguo Xu[3]

J. Electrical Systems 15-1 (2019): 81-95

Regular paper

A New Robust Control for Grid Connected Photovoltaic Systems Based on Active Disturbance Rejection Control

The aim of this study is to improve the stability performance of grid connected photovoltaic (PV) systems with LCL filters. PID controllers are commonly used in these systems but they are not well adapted to parameters uncertainties, sudden change in the climate conditions and disturbances. This paper proposes an alternative robust control strategy to ensure the maximum extraction of the available power and the efficient transfer of the solar energy to the grid by using the active disturbance rejection control. This control technique provides better performances by increasing the system efficiency and ensuring stability under parameter variations and disturbances. Moreover, the LCL filter resonance is actively damped with a minimum complexity in the controller design, and without any adaptive algorithm. The effectiveness of the proposed control is demonstrated through simulation results, in which its performance is shown to be superior to that of the conventional PID controller.

Keywords: PV system, grid-connected inverter, ADRC, Active damping, LCL filter.

Article history: Received 29 April 2018, Accepted 17 January 2019

1. Introduction

The interconnection of photovoltaic (PV) power systems with the utility grid has been continuously increasing during the last few years. Moreover, due to the still decreasing installation costs, PV systems are expected to play an even more significant role in the future power generation [1], [2].

In grid connected applications, the PV source is connected to the grid through power electronics interface, where the two-stage topology is commonly used [3]. Figure 1 shows such a topology, which offers more flexibility in term of controllability. The first stage extracts the maximum solar energy by implementing an MPPT controller in cascade with a voltage regulator to mitigate load and environmental disturbances. The second stage ensures the efficient transfer of the energy to the grid [3]. The LCL filter is incorporated between the inverter and the grid due to its high attenuation of switching harmonics injected into the grid [4].

Following the stability issues caused by the resonance phenomena of LCL filters, the control design of these resonant filters becomes very challenging. Many damping methods have been proposed to deal with this problem [4, 5]. Passive damping methods can absorb the resonance effectively and maintain system stability but its performance is inevitably limited by additional power losses [6]. Consequently, active damping methods are preferred by simply adding a digital filter to the current controller [7] or based on the state feedback controller [8-10]. However, all these controllers are based on the detailed model of the system, and then any discrepancy between the real model and the calculated model may

* Corresponding author: A. Benrabah, Electrical Engineering Department, Ecole Militaire Polytechnique, 16000 Algiers, Algeria, E-mail: benrabah.abdeldjabar@hit.edu.cn

[1] Electrical Engineering Department, Ecole Militaire Polytechnique, 16111 Algiers, Algeria

[2] Department of Electrical Engineering, University of Lahore, 54000 Lahore, Pakistan

[3] School of Electrical Engineering and Automation, Harbin Institute of Technology, 150001 Harbin, China

Copyright © JES 2019 on-line: journal/esrgroups.org/jes

lead to system instability. In fact, the presence of disturbances and parameter uncertainties may compromise the stability of these controllers.

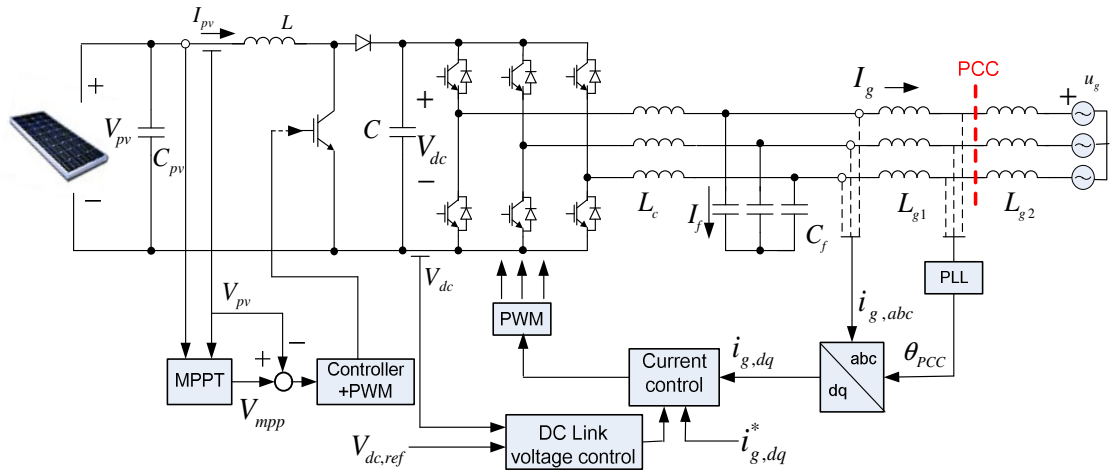

Figure 1. Two-stage topology of grid tied photovoltaic system

In practical operations, a high performance of the photovoltaic system is required, such as a smooth and fast response, and a strong robustness under internal and external disturbances and uncertainties. All of them are dependent on the control performance of the power electronic converter to a great extent. Therefore, the power electronic converter control plays a decisive role on the whole performance of the PV system. Proportional-Integral-Derivative (PID) controller is a simple and universal control method which has been used in a wide variety of control areas. However, for a nonlinear and discontinuous system such as the power converter, the results of the PID controller are usually unsatisfactory [8, 11]. In recent years, some other advanced control strategies, such as adaptive control, fuzzy logic, feedback linearization techniques, have also been applied for power electronic converters control [12–14]. However, they either require too complex computations or have strict requirements for an accurate mathematical model of the system, both of which are very difficult to obtain in reality [11]. In the last few years, a promising new technology named Active Disturbance Rejection Control (ADRC) has been explored in almost all domains of control engineering as an attractive alternative over conventional PID and model-based controls [15, 16]. The ADRC has been recognized as an effective control method in dealing with dynamic uncertainties and disturbances without needing an explicit model of the plant. Robust stability analysis of the ADRC based-control systems has been performed and presented in [17].

In this paper, the ADRC technique is applied to improve the stability performance of PV systems connected to the grid through an LCL filters. The power electronic converter in this system is made up of a DC-DC boost converter in cascade with a three-phase current controlled grid connected inverter. Various case studies are conducted to verify the effectiveness of the proposed controller comparing with the traditional PI controller.

The remainder of this paper is organized as follows. The ADRC technique theory is presented in Section 2. The PV side converter and the grid side converter controls are provided in Section 3 and 4 respectively. The tuning process is presented in Section 5.

Simulation results and discussion are given in Section 6. Finally, Section 7 is devoted to some concluding remarks.

2. Brief summary of ADRC

Consider the n^{th} order process with single input u and single output y described as

$$\begin{cases} x^{(n)} = f(t, x, \dot{x}, ..., x^{(n-1)}, d) + bu \\ y = x \end{cases} \tag{1}$$

It can be also described as

$$\begin{cases} \dot{x}_1 = x_2 \\ . \\ . \\ \dot{x}_{n-1} = x_n \\ \dot{x}_n = f(x_1, x_2, ..., x_{n-1}, d) + bu \\ y = x_1 \end{cases} \tag{2}$$

where b is a system parameter and $f(.)$ represents the total disturbance including the internal dynamics and disturbances. Without an explicit model of the plant, the ADRC is able to control the system output and ensure system stability by compensating the total disturbance [16, 18].

The main idea of the ADRC is to treat the model uncertainties and disturbances as total disturbance, then estimate it in real time and compensate its effect. As shown in Figure 2, this control involves two control loops. The inner loop is designed to reject the total disturbance while the outer loop aims to generate the desired signal by using a feedback controller.

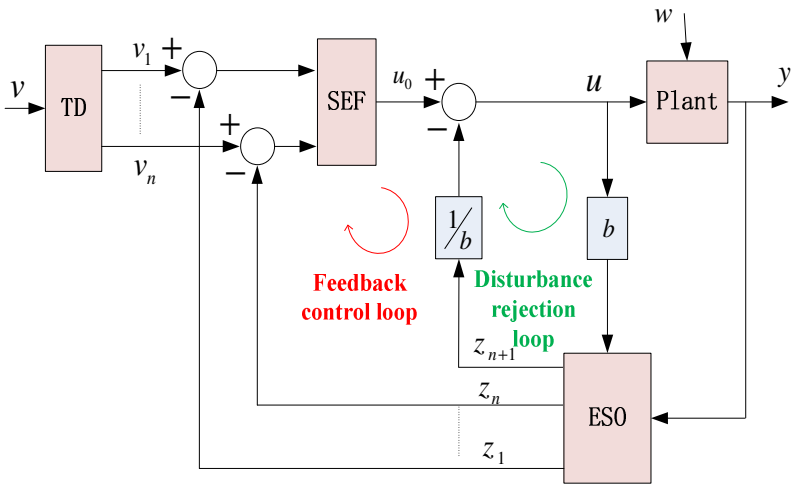

Figure 2. Block Diagram of ADRC Controller

ADRC involves three main blocks: the tracking differentiator (TD), the extended state observer (ESO), and the state error feedback control law (SEF), which will be simply introduced as follows.

TD is used to arrange the transient process and conveys each order derivative of the input signal. It is expressed by

$$\begin{cases} \dot{v}_1 = v_2 \\ \dot{v}_2 = v_3 \\ . \\ . \\ \dot{v}_{n-1} = v_n \\ \dot{v}_n = r^n \psi(v_1 - v, \frac{v_2}{r}, ..., \frac{v_n}{r^{n-1}}) \end{cases} \tag{3}$$

where v is the input signal, $v_i\,(i = 1, 2, \ldots, n)$ is the output, r is the adjustable speed factor and $\psi(.)$ is a nonlinear function.

The ESO is the core part of the ADRC. It is used to estimate the object's state variables and the total disturbance. The mathematical model for the nonlinear ESO is as follows

$$\begin{cases} e = z_1 - y \\ \dot{z}_1 = z_2 - \beta_{01} e \\ \dot{z}_2 = z_3 - \beta_{02}\, fal(e, \alpha_{02}, \delta) \\ .. \\ \dot{z}_n = z_{n+1} - \beta_{0n}\, fal(e, \alpha_{0n}, \delta) + bu(t) \\ \dot{z}_{(n+1)} = -\beta_{0(n+1)}\, fal(e, \alpha_{0(n+1)}, \delta) \end{cases} \tag{4}$$

where $z_i\,(i = 1, 2, \ldots, n+1)$ are the observer outputs, $\beta_{0i}\,(i = 1, 2, \ldots, n+1)$ are the observer gains, and e is the estimation error . $fal(.)$ is a nonlinear function defined as

$$fal(x, \alpha, \delta) = \begin{cases} |x|^{\alpha}\, sign(x), |x| > \delta \\ x / \delta^{1-\alpha}, |x| \le \delta \end{cases} \tag{5}$$

where α and δ are two design parameters.

The nonlinear state error feedback (SEF) uses a nonlinear algorithm of the control error to generate the control input u_0:

$$\begin{cases} e_1 = x_1 - z_1 \\ e_2 = x_2 - z_2 \\ .. \\ e_n = x_n - z_n \\ u_0 = \beta_1 fal(e_1, \alpha_1, h) + \beta_2 fal(e_2, \alpha_2, h) + ... + \beta_n fal(e_n, \alpha_n, h) \end{cases} \tag{6}$$

where $e_i\,(i = 1, 2, \ldots, n)$ are the control errors, $\alpha_i\,(i = 1, 2, \ldots, n)$, $\beta_i\,(i = 1, 2, \ldots, n)$ and h are adjusting parameters.

Finally, the system control law u is given by

$$u = u_0 - \frac{z_{n+1}}{b},\ i = 1, 2, \ldots, n. \tag{7}$$

3. PV side boost converter control

Figure 3 shows a simplified circuit of a step-up DC-DC converter commonly used to boost the output PV voltage to the high DC-input voltage of the inverter [3, 19]. The DC-link voltage regulation is performed by the outer control loop of the grid connected inverter.

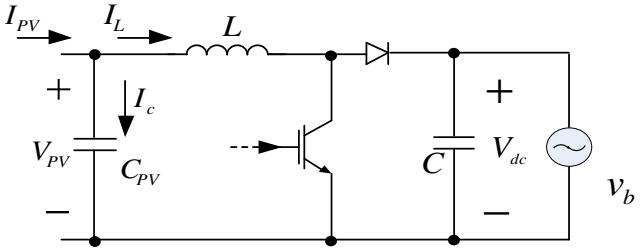

Figure 3. Boost switching converter used in PV system

The main objective of the PV side converter control is to extract the maximum power available from the source by using the maximum power point tracking (MPPT) control. There are a lot of MPPT algorithms proposed in literature [2, 20], among these, the Perturb and Observe (P&O) algorithm based on the PV voltage regulation, has gained a great attention due to its efficiency and simplicity.

In order to improve the control capability, the voltage closed-loop must be designed to ensure fast dynamic response with respect to the reference signal defined by the P&O algorithm and to reject efficiently the disturbances at input and output of the DC-DC converter. This can be achieved by using the ADRC controller.

Applying Kirchhoff laws to the scheme in Figure 3 leads to (8)

$$i_{PV} = i_C + i_L \tag{8}$$

By replacing the capacitor current and the photovoltaic current in (8), the equation (9) is obtained.

$$\frac{dV_{PV}}{dt} = \frac{1}{C_{pv}R_{pv}}V_{PV} - \frac{1}{C_{pv}}i_L \tag{9}$$

with $V_{pv} = R_{pv}I_{pv}$

Let $y=V_{PV}$ be the state variable. The equation (9) can be rewritten as

$$\dot{y} = f(t, \dot{y}) + bu \tag{10}$$

where $b = -1/C$, u is the control input and $f(.)$ is the total disturbance.

The second order ESO is expressed as follows:

$$\begin{cases} e = z_1 - y \\ \dot{z}_1 = z_2 - \beta_{01} fal(e, \alpha_{01}, \delta) + bu(t) \\ \dot{z}_2 = -\beta_{02} e \end{cases} \tag{11}$$

The SEF expression is given by

$$\begin{cases} e_1 = V_{mpp} - z_1 \\ u_0 = \beta_1 fal(e_1, \alpha_1, h) \end{cases} \tag{12}$$

The control signal then can be built according to the following equation

$$u = u_0 - \frac{z_2}{b} \tag{13}$$

The control scheme of the ADRC based MPPT system for a photovoltaic array using DC-DC boost converter is shown in Figure 4.

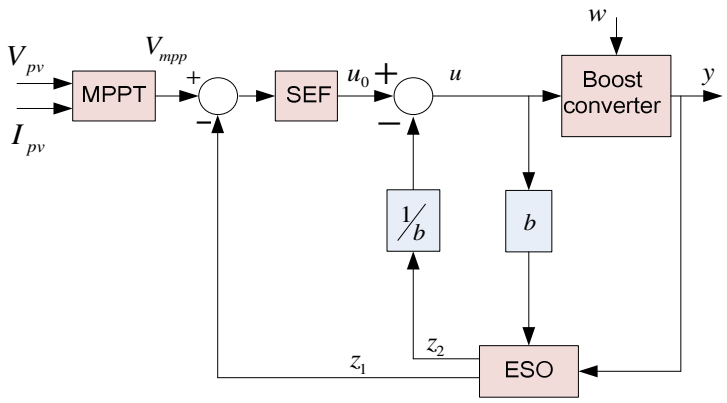

Figure 4. ADRC Based MPPT control of boost converter

4. Grid side control

The voltage source inverter (VSI) control is realized through two main control loops as depicted in Figure 1. The internal loop is responsible for grid current control and resonance damping while the external loop is responsible for DC-link voltage control and generating the active current reference corresponding to the active power exchanged with the grid.

4.1. DC-link voltage controller

In order to improve the voltage regulation, the ADRC controller is applied to control the DC-link voltage as shown in Figure 5.

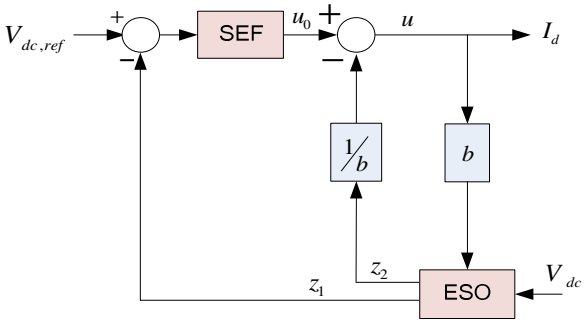

Figure 5. ADRC controller for DC voltage control

The control is formulated in the ADRC framework as follows

$$C\frac{dV_{dc}}{dt} = I_{pvs} - I_d \tag{14}$$

$$\frac{dV_{dc}}{dt} = \frac{1}{C}I_{pvs} - \frac{1}{C}I_d = f(t) + bu \tag{15}$$

where V_{dc} is the system output, I_d is the controlled variable, I_{pvs} is the output current of the solar energy which is considered as a disturbance in this system.

The extended state observer is given by

$$\begin{cases} e = z_1 - V_{dc,ref} \\ \dot{z}_1 = z_2 - \beta_{01} fal(e, \alpha_{01}, \delta) - \frac{1}{C} I_d \\ \dot{z}_2 = -\beta_{02} e \end{cases} \tag{16}$$

The nonlinear SEF and the control law are expressed in equation (16) and (17) respectively

$$\begin{cases} e_1 = V_{mpp} - z_1 \\ u_0 = \beta_1 fal(e_1, \alpha_1, h) \end{cases} \tag{17}$$

$$u = u_0 - \frac{z_2}{b} \tag{18}$$

4.2. Grid current control

To deal with parameter uncertainties and disturbances, the *LCL* filtered VSI requires an advanced control strategy in order to maintain a better stability performance. Moreover, the presence of the *LCL* filter will create a resonance problem which needs to be passively or actively damped to ensure the system stability. A new robust approach is proposed in this work by using the ADRC based active damping control.

The grid current can be expressed in the s-domain by

$$i_g(s) = \frac{v_c(s) + (L_c C_f s^2 + r_c C_f s + 1) v_g(s)}{L_c L_g C_f + (r_c L_g C_f + r_g L_c C_f) s^2 + (L_c + L_g + r_c r_g C_f) s + r_c r_g} \tag{19}$$

In order to apply the ADRC, (19) is reformulated as

$$\begin{cases} i_g = x_1 \\ \dot{i}_g = x_2 \\ \ddot{i}_g = x_2 \\ y = i_g \end{cases} \tag{20}$$

where

$$\begin{cases} \dot{x}_1 = x_2 \\ \dot{x}_2 = x_3 \\ \dot{x}_3 = \dfrac{1}{L_c L_g C_f}(-(r_c L_g C_f + r_g L_c C_f)x_3 - (L_c + L_g + r_c r_g C_f)x_2 \\ \qquad - r_c r_g x_1 + v_c + L_c C_f \ddot{v}_g + r_c C_f \dot{v}_g + v_g) \\ y = x_1 \end{cases} \tag{21}$$

This can be written in the state space form as

$$\begin{cases} \dot{x}_1 = x_2 \\ \dot{x}_2 = x_3 \\ \dot{x}_3 = f(x_1, x_2, x_3, d) + bu \\ y = x_1 \end{cases} \tag{22}$$

where y is the output, u is the input, and f is the total disturbance including the resonance and other unmodeled dynamics.

Figure 6 shows the grid-connected inverter control scheme where the ADRC-based control system is treated as two single-input single-output (SISO) subsystems. The active and reactive current are controlled independently so that the cross-coupling terms are also considered as part of the total disturbance. Each SISO controller is assigned to one of the *dq* current components and involves a third order TD, a fourth order ESO, and nonlinear SEF.

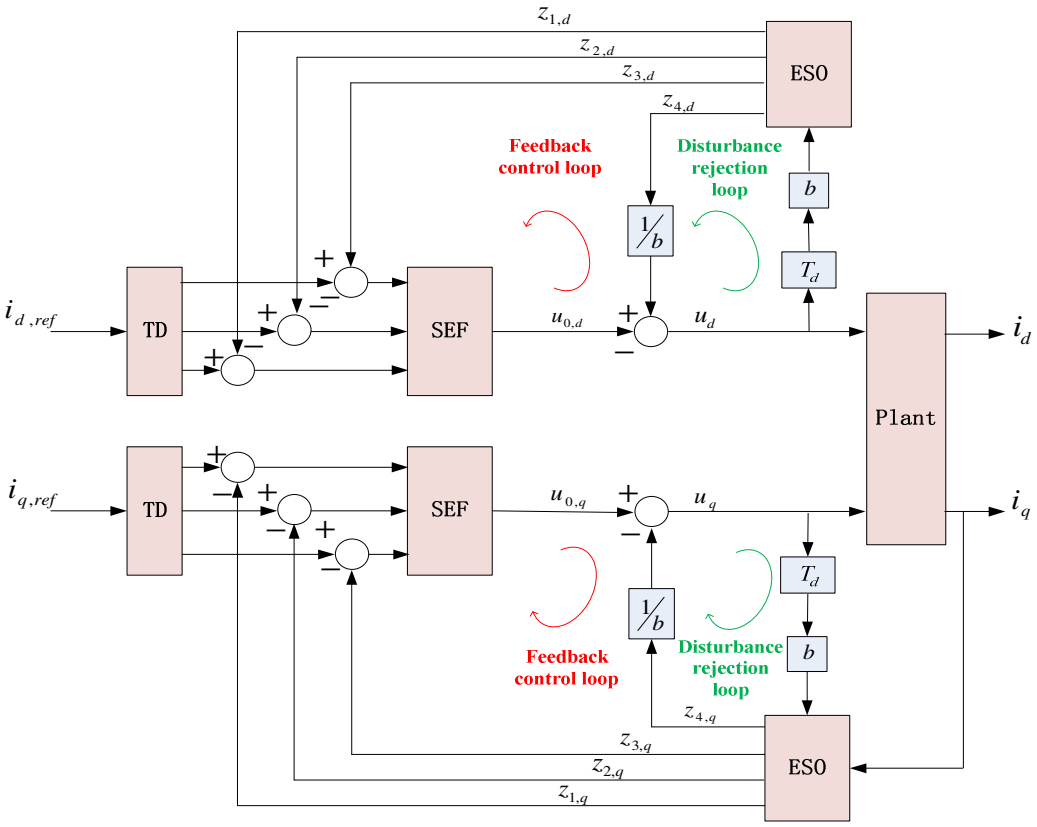

Figure 6. Grid connected inverter current control based on ADRC

The third order TD is obtained by connecting two second order TDs in series as follows

$$\begin{cases} \dot{x}_1 = v_2 \\ \dot{v}_2 = fhan(x_1 - v_1, v_2, r_1, h_1) \\ \dot{x}_2 = x_3 \\ \dot{x}_3 = fhan(x_2 - v_2, x_3, r_2, h_2) \end{cases} \tag{23}$$

where r_1, r_2 and h_1, h_2 are the speed factors, and the filtering factors of TD_1 and TD_2 respectively.

The SEF can be written as

$$\begin{cases} e_1 = x_1 - z_1 \\ e_2 = x_2 - z_2 \\ e_3 = x_3 - z_3 \\ u_0 = \beta_1 fal(e_1, \alpha_1, h) + \beta_2 fal(e_2, \alpha_2, h) + \beta_3 fal(e_3, \alpha_3, h) \end{cases} \tag{24}$$

The ESO is expressed as follows

$$\begin{cases} e = z_1 - y \\ \dot{z}_1 = z_2 - \beta_{01} e \\ \dot{z}_2 = z_3 - \beta_{02} fal(e, \alpha_{02}, \delta) \\ \dot{z}_3 = z_4 - \beta_{03} fal(e, \alpha_{03}, \delta) + bu(t - T_d) \\ \dot{z}_4 = -\beta_{04} fal(e, \alpha_{04}, \delta) \end{cases} \tag{25}$$

Compared with a regular design, a time delay T_d is inserted before the ESO to delay the control input u. In this manner, the observer makes use of the delayed input and gives synchronized estimation of the delayed states and disturbances since the control output is already delayed due to the system dynamics [16, 21].

Finally, the control law is obtained by

$$u = u_0 - \frac{z_4}{b} \tag{26}$$

5. Tuning methodology

The considered system controllers were tuned empirically with the goal to provide the best control quality. It is worth noting that the ESO and the SEF are designed separately but the ESO should be tuned first since the ESO is in inner loop while the SEF is in the outer loop.

In the TD, we can get different transient processes by regulating the speed factor r and the filtering factor h. When r is larger, the transition process will be faster but the noise will be significant. Additionally, increasing h can improve the filter properties. In the case of the first order process, TD is not used since the derivative of the signal is not needed.

In the ESO, the observer gains and functions in (4) must be tuned adequately to get the accurate estimations of the system states and disturbances. The best way is to adjust the observer gains β_{0i} first and then monotonously increase the nonlinearity by tuning α_{0i} and δ. Once the ESO is correctly tuned, the obtained estimates are quite insensitive to parameters variations and disturbances.

Finally, the nonlinear SEF play important role in improving the control performances and rejecting disturbances [22]. In fact, the SEF is a flexible tool to simultaneously achieve multiple design requirements. As an example, third order SEF is designed by tuning $0 < \alpha_1 < 1$ to improve the tracking performance, $0 < \alpha_2 < 1$ to prevent integration windup and $\alpha_3 > 1$ to reduce the overshoot. In practice, using integral or derivative actions depends on control requirements.

6. Performance evaluation results

This section is devoted to verify the effectiveness of the proposed controller and compare its performance with the conventional PI-based control under the same conditions. The power system links a 12kW photovoltaic array to the utility grid. The solar array was modelled according to the parameters taken from BP 7180 module of BP Solar. In order to obtain a 12kW PV's generated power; ten subarrays of 6 BP 7180 module series string were connected in parallel. The parameters of one BP 7180 solar module are summarized in Table 1. The operation temperature of the PV source is considered constant at 25 °C in all performed simulations. Matlab simulations of the complete system with the proposed controllers have been carried out using the parameters given in Table 2. The direct current component i_d is made by outer DC-link voltage control loop and the quadrature current component i_q is forced to be zero to minimize the injected reactive power to the grid. A passive damping resistor is added in series with the filter capacitor when using the PI controller to address the resonance problem of the *LCL* filter, because without any damping, the PI control cannot ensure the system stability.

Table 1: Electric characteristics of solar array BP Solar BP7180S

Parameters	VALUE
Maximum power (P_{max})	180W
Operating Voltage (V_{mpp}) at(P_{max})	36.2 V
Operating Current at (I_{mpp}) at(P_{max})	5 A
Short-circuit Current (I_{SC})	5.4 A
Open circuit voltage (V_{OC})	44.8 V
Temperature coefficient of (I_{SC})	(0.065±0.015) %/K
Temperature coefficient of (V_{OC})	-(160±10) mV/K

Table 2: Parameters of the considered system

Parameters	VALUE
Parameters	Value
PV capacitance (C_{pv})	10 µF
Boost Inductance (L)	100 mH
DC-Link capacitance (C)	1000 µF
Converter side inductance (L_c)	4 mH
Grid side inductance (L_g)	[1.5,2.5] mH
Filter capacitance (C_f)	10 µF
DC-Link voltage (V_{dc})	800 V
Grid voltage L-N (v_g)	240 V
Frequency of grid voltage (f)	50 Hz
Switching/Sampling frequency	10 kHz

In order to demonstrate the benefits of the proposed MPPT-ADRC controller over the MPPT-PI based controller, Figure 7 shows the comparison results of the PV current responses under sudden variations of sun irradiation. As can be seen, the MPPT controller ensure global stability in both control methods but the ADRC-based control exhibit a much faster response leading to smaller oscillation and more energy extracted from the PV source. Moreover, it is shown that under large variations of sun irradiation, the ADRC-based control compensates with higher efficiency the perturbations in comparison with the PI-based control. The difference between the two responses is explained by the fact that in the P&O algorithm, the sampling time should be larger than the settling time to maintain system stability. In the case of the PI-based control, the settling time changes with solar irradiance variations, then the sampling time must be set to the worst case exhibited by the system to keep the system stable (longest sampling time). On the contrary, the proposed ADRC-based control with a model free tuning method provides a constant settling time, shorter than the PI controller settling time, which in turn enhance the controller performance by reducing the power losses as illustrated in Figure 8.

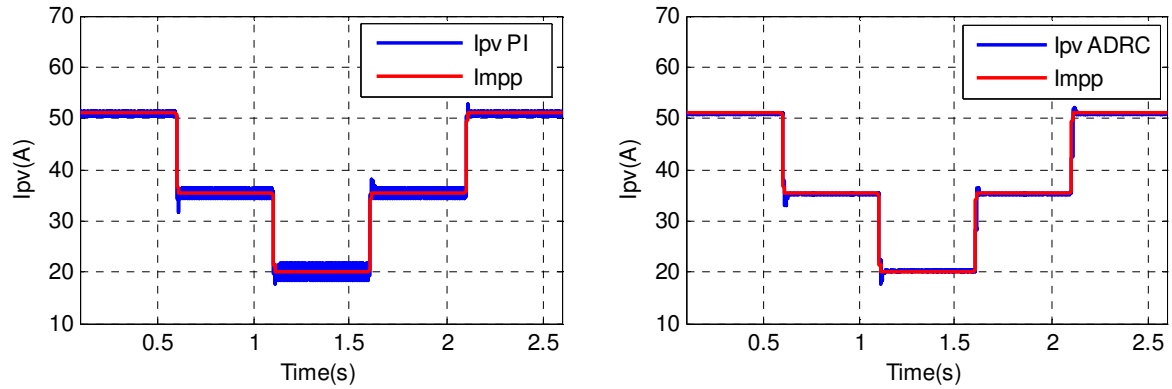

(a) (b)

Figure 7. Comparison results of the PV current. (a) PI control, (b) ADRC control

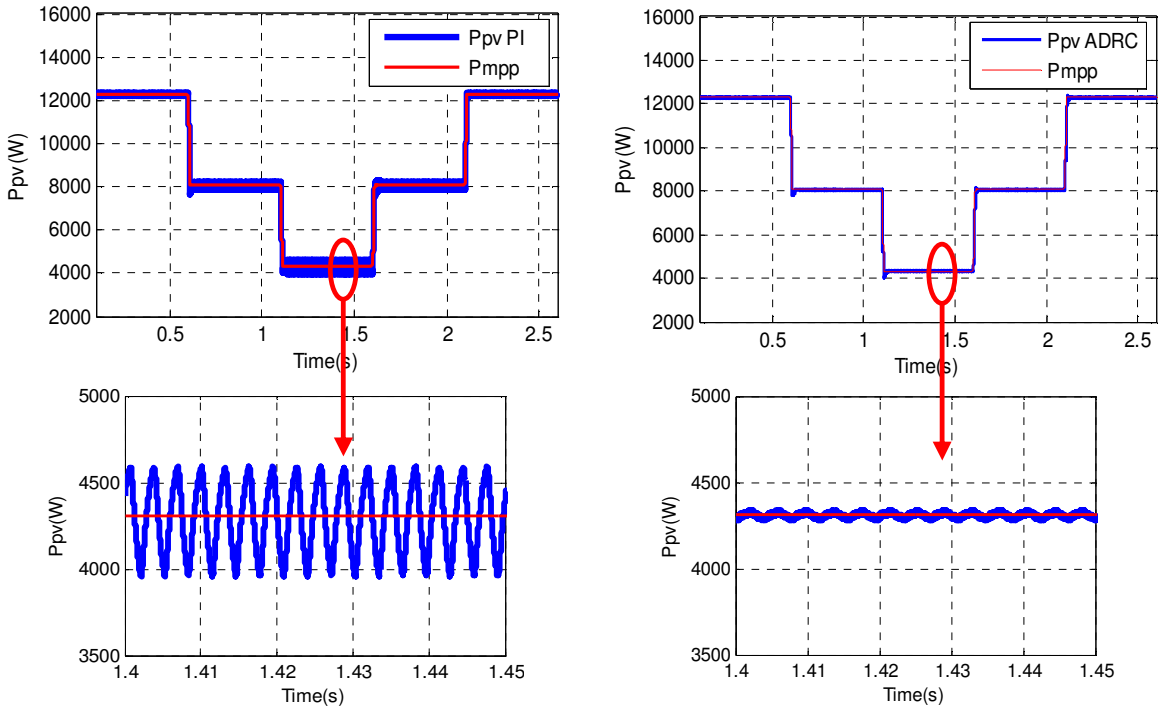

(a) (b)

Figure 8. Comparison results of the PV power. (a) PI control, (b) ADRC control

Figure 9 illustrates the response of the DC-link voltage controller during sun irradiation fluctuations. As can be seen, the DC-link voltage acts differently. Obviously, in the case of the ADRC controller, the DC-voltage exhibits less overshoot and faster response compared to PI regulator.

Figure 10(a) and 10(b) illustrate the response of the closed-loop current controller for step changes of solar irradiance and the capability of the designed current controller to independently control the injected active and reactive power by using the active disturbance rejection control. As can be seen, the LCL filter resonance is actively damped and the closed-loop current controller closely tracks the generated current reference after sudden change of the active power due to the climate conditions.

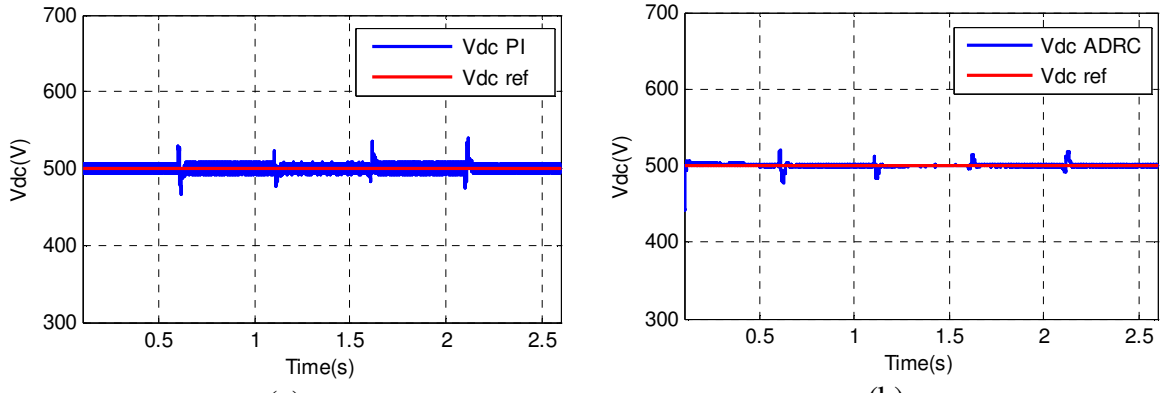

(a) (b)

Figure 9. DC link voltage response. (a) PI control, (b) ADRC Control

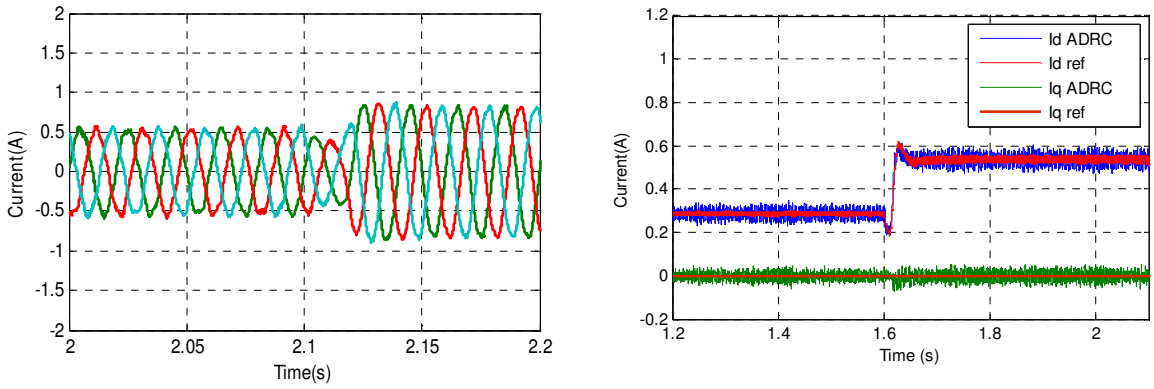

(a) (b)

Figure 10. Transient response after a sudden change of solar irradiance. (a) Three phase grid currents, (b) Grid dq axis current reference tracking

To investigate the robustness of the ADRC controller under parameters variation, the effect of changing the output filter inductance value on the output current has been evaluated. Figure 11(a) shows the evolution of the grid current after a 2 *pu* variation in the grid side inductance L_g. This variation has almost no influence on the system stability because the ADRC automatically compensates the resonance even under parameter variations. However, without passive damping, the PI controller-based control loses stability due to the *LCL* filter resonance as shown in Figure 11(b).

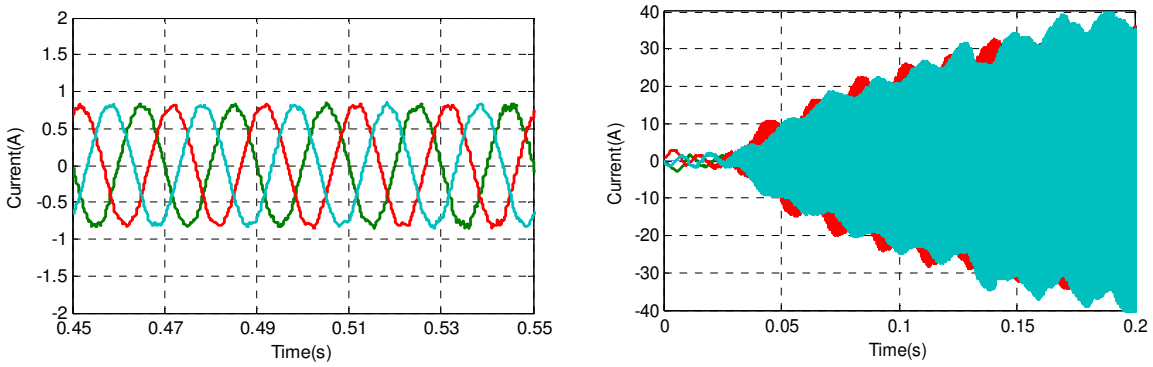

(a) (b)

Figure 11. Robust stability performance. (a) Stable performance of the ADRC under grid inductance variation, (b) Unstable performance of the PI control without passive damping

In order to analyse the complete effectiveness of the proposed control method, the proposed controller is evaluated in the presence of grid voltage disturbances: 5% of the 5th harmonic and 3% the 7th harmonic. The harmonic analysis of the grid current in Figure 12(a) shows the high-quality current injection even under grid voltage disturbances with a THD of 2.21%. The grid current harmonic content is reduced below the acceptable limits allowed by IEEE Std.1547. Figure 12(b) shows that the proposed control still ensures good tracking of the grid current reference as the grid disturbances have been successfully rejected by the active disturbance rejection control leading to high and robust stability performance.

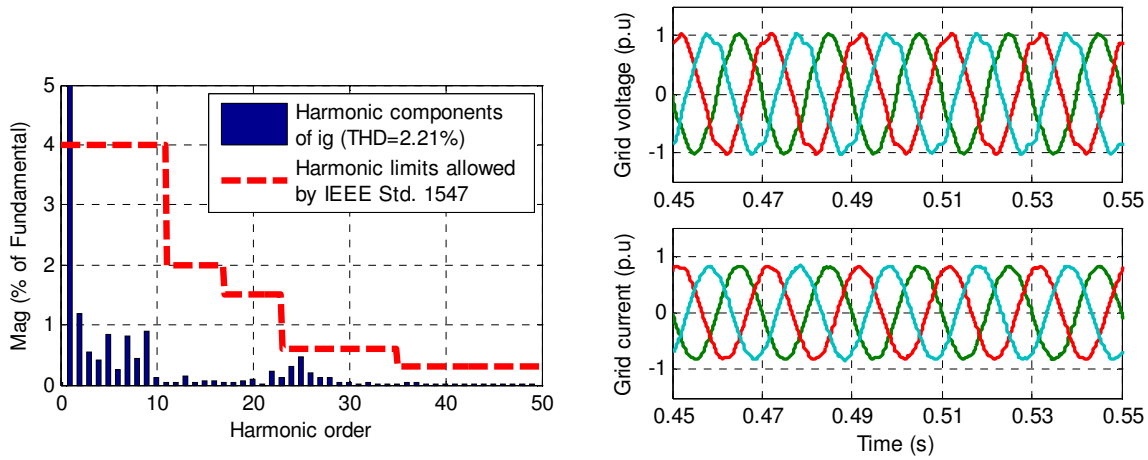

(a) (b)

Figure 12. Grid disturbance rejection ability of the proposed ADRC controller. (a) Harmonic analysis of injected grid current, (b) Grid voltage and grid current responses under grid disturbances

7. Conclusion

An active disturbance rejection control for grid-connected PV systems is presented in this paper. First, the MPPT controller of the boost converter was enhanced by including the ADRC technology which provides a notable efficiency, since it permits to track the optimum power quickly despite the atmosphere condition changing. Secondly, the ADRC technique was applied for LCL filtered grid connected inverter control. The controller shows strong robustness under parameter variations and the LCL filter resonance was actively damped without the need for additional sensors and without any adaptive algorithm. The good performance of this new robust control was verified with time-domain simulation studies that are illustrated with rapid changes in solar irradiance and parameter variations. Simulations results were contrasted with the conventional PI controller to highlight the advantages of the proposed solution.

References

[1] Mahamat C, Petit M, Costa F, Marouani R, Mami A. Optimized Design of an LCL Filter for Grid Connected Photovoltaic System and Analysis of the Impact of Neighbors' Consumption on the System. Journal of Electrical systems, 2017, 13(4), 618–632.

[2] Chao R M, Ko S H, Lin H K, Wang I K, Evaluation of a Distributed Photovoltaic System in Grid-Connected and Standalone Applications by Different MPPT Algorithms. *Energies*, 2018, 11(6): 1484–1490.

[3] Trejos A, Gonzalez D, Ramos-Paja C A. Modeling of step-up grid-connected photovoltaic systems for control purposes. *Energies*, 2012, 5: 1900–1926.

[4] Wu W, Liu Y, He Y, Chung H S, Liserre M, and Blaabjerg F. Damping methods for resonances caused by LCL-filter-based current-controlled grid-tied power inverters: An overview. *IEEE Transactions on Industrial Electronics*, 2017, 64(9), 7402–7413.

[5] Saïd-Romdhane M B, Naouar M W, Slama-Belkhodja I, Monmasson E. Robust active damping methods for LCL filter-based grid-connected converters. *IEEE Transactions on Power Electronics*, 2017, 32(9): 6739–6750.

[6] Peña-Alzola R, Liserre M, Blaabjerg F, Sebastián R, Dannehl J, Fuchs F W. Analysis of the passive damping losses in LCL-filter-based grid converters. *IEEE Transactions on Power Electronics*, 2013, 28(6): 2642–2646.

[7] Yao W, Yang Y, Zhang X, Blaabjerg F, Loh P C. Design and analysis of robust active damping for LCL filters using digital notch filters. *IEEE Transactions on Power Electronics*, 2017, 32(3): 2360–2375.

[8] Said-Romdhane M B, Naouar M W, Slama-Belkhodja I, Monmasson E. Robust Active Damping Methods for LCL Filter Based Grid Connected Converters. *IEEE Transactions on Power Electronics*, 2017, 32(9):6739-6750.

[9] Xin Z, Wang X, Loh P. C, Blaabjerg F. Grid-current-feedback control for LCL-filtered grid converters with enhanced stability. *IEEE Transactions on Power Electronics*, 2017, 32(4):3216-3228.

[10] Pan D, Ruan X, Bao C, Li W, Wang X. Capacitor-current feedback active damping with reduced computation delay for improving robustness of LCL-type grid-connected inverter. *IEEE Transactions on Power Electronics*, 2014, 29(7): 3414–3427.

[11] Sun B, Gao Z. A DSP-based active disturbance rejection control design for a 1-kW H-bridge DC-DC power converter. *IEEE Transactions on Industrial Electronics*, 2005, 52(5): 1271–1277.

[12] Zhao J, Liu Y, Qu K, Geng H. Adaptive hysteresis band control for DC-DC buck converter. In: IEEE Energy Conversion Congress and Exposition, 2013: 804–809.

[13] Fei J, Zhu Y. Adaptive fuzzy sliding control of single-phase PV grid-connected inverter. *PLoS ONE*, 2017, 12(8): e0182916.

[14] Bao X, Zhuo F, Tian Y, Tan P. Simplified feedback linearization control of three phase photovoltaic inverter with an LCL filter. *IEEE Transactions on Power Electronics*, 2013, 28(6): 2739–2752.

[15] Benrabah A, Xu D, and Gao Z. Active Disturbance Rejection Control of LCL-Filtered Grid Connected Inverter Using Padé Approximation. *IEEE Transactions on Industry Applications*, 2018, 54(6): 6179-6189.

[16] Han J. From PID to active disturbance rejection control. *IEEE Transactions on Industrial Electronics*, 2009, 56(3): 900–906.

[17] Qi X, Li J, Xia Y, et al. On the robust stability of active disturbance rejection control for SISO systems. *Circuits, Systems, and Signal Processing*, 2017, 36(1): 65–81.

[18] Tang H, Li Y. Development and active disturbance rejection control of a compliant micro-nano-positioning piezostage with dual mode. *IEEE Transactions on Industrial Electronics*, 2014, 61(3): 1475–1492.

[19] Femia N, Petrone G, Spagnuolo G, Vitelli M. A technique for improving P&O MPPT performances of double-stage grid-connected photovoltaic systems. *IEEE Transactions on Industrial Electronics*, 2009, 56: 4473–4482.

[20] Esram T, Chapman P L. Comparison of photovoltaic array maximum power point tracking techniques. *IEEE Transactions on Energy Conversion*, 2007, 22:439–449.

[21] Zhao S, Gao Z. Modified active disturbance rejection control for time-delay systems. *ISA Transactions*, 2014, 53(4): 882–888.

[22] Xia Y, Fu M. Overview of ADRC. in Compound Control Methodology for Flight Vehicles, *Lecture Notes in Control and Information Sciences*, 2013, 438:21–48.